Surface & Coatings Technology 473 (2023) 129911

Contents lists available at ScienceDirect

Surface & Coatings Technology

journal homepage: www.elsevier.com/locate/surfcoat

Effect of oxidation temperature on the properties of niobium in view of its biomedical applications

Tomasz Borowski [a,*], Katarzyna Zielińska [a], Maciej Spychalski [a], Bogusława Adamczyk-Cieślak [a], Łukasz Żrodowski [a,b]

[a] Warsaw University of Technology, Faculty of Materials Science and Engineering, Warsaw, Poland
[b] AMAZEMET Ltd, Al. Jana Pawła II 27, 00-867 Warsaw, Poland

ARTICLE INFO

Keywords:
Niobium
Oxidation
Microstructure
Corrosion
Contact angle
Surface engineering

ABSTRACT

Four-hour oxidation processes of niobium in an air atmosphere at temperatures of 400 °C, 425 °C, 450 °C and 500 °C were carried out. In order to characterise the layers produced, the cross-sectional microstructure, chemical and phase composition as well as surface roughness were examined. The mechanical properties of the surface were determined by performing Vickers microhardness tests. In order to verify the properties from a biological point of view, contact angle analysis and corrosion tests in Ringer's solution were carried out. The results revealed the formation of layers composed of a solid solution of oxygen in niobium Nb(O) at oxidation temperatures of 400 °C, a solution of Nb(O) and niobium pentoxide Nb_2O_5 at 425 °C, and Nb_2O_5 at 450 °C and 500 °C. Increased oxidation temperature resulted in an increase in hardness and surface roughness, and each process contributed to improved corrosion resistance. Oxidation at too high temperature (≥450 °C) caused degradation of the material's surface due to niobium's low heat resistance. At 450 °C the first cracks in the material were visible, and at 500 °C the layer was inhomogeneous, brittle and underwent significant chipping. The highest hardness, roughness and hydrophobic properties were shown by niobium oxidised at 500 °C, which underwent surface degradation at this temperature. In turn, niobium oxidised at 400 °C and 425 °C showed outstanding properties in the biological aspect, achieving both high hydrophilicity and the highest corrosion resistance.

1. Introduction

Currently, metallic materials are the most common type of materials used in medical applications. Unfortunately, developing a material that will not corrode in the environment of the human body often poses a problem. The occurrence of corrosion can cause both a decrease in the mechanical properties of the material and entry of dangerous ions into the body (metallosis). It is claimed that the more corrosion-resistant the material, the more biocompatible it is [1]. The type of metal surface which comes in direct contact with human body tissue strongly determines its qualification as a biomaterial. In order to improve biological properties, a layer of metal oxides (TiO_2, ZrO_2) is often used. Niobium oxide is also an example of such a material. It is usually deposited on various alloys in the form of coatings by different surface engineering methods, including flame spraying [2], DC magnetron sputtering [3], reactive sputtering [4], electron beam deposition [5] or plasma spraying [6]. This material is characterised by very high corrosion resistance, thermodynamic stability and high biocompatibility [7]. Wadullah et al. [8] fabricated a nano-layer of Nb_2O_5 by synthesizing it on the surface of a Ni-Cr-Mo alloy using the hydrothermal technique. The results showed a significant improvement in the corrosion resistance of a surface coated with a thin layer of Nb_2O_5 compared to an uncoated surface. In another paper by Pauline et al. [9], a niobium oxide layer was deposited on the surface of AISI 316L steel by the sol-gel method using the spin coating technique. The resulting coating achieved high hardness, good adhesion, and improved corrosion resistance compared to the starting material. In addition, some studies have shown that osteoblast adhesion and proliferation on an Nb_2O_5 coating produced on AISI 316 steel are comparable to TiO_2 [10]. In turn, the work of Eisenbarth et al. [11] observed that cp-Ti titanium coated with niobium oxide showed increased migration and adhesion of MC3T3-E1 cells compared to uncoated titanium. As can be seen from the above literature, biocompatible Nb_2O_5 coatings are successfully obtained on various alloys; however, there is a small amount of work on the production and testing of oxide

* Corresponding author.
E-mail address: tomasz.borowski@pw.edu.pl (T. Borowski).

https://doi.org/10.1016/j.surfcoat.2023.129911
Received 2 June 2023; Received in revised form 4 August 2023; Accepted 9 August 2023
Available online 10 August 2023

films in oxidation processes of pure niobium [12–15], especially those obtained by thermal methods [16]. Niobium is widely used in aerospace, superconducting magnet production, defense, the nuclear industry and electronics manufacturing [17–19]. Nb-based materials have been shown to be hypoallergenic and biologically safe, as they are tolerated by the human body [20]. Eisenbartha et al. [21] studied pure niobium (cp-Nb), showing that cell proliferation, mitochondrial activity and cell volumes were similar compared to titanium and better than stainless steel, with the conclusion that further research on niobium and its oxides is worth pursuing. Canepa et al. [22] studied the growth of an anodic oxide layer on niobium in a Ca and P-containing electrolyte as a function of the anodizing potential. At higher potentials, they observed thicker and microporous oxide layers, with significant enrichment in Ca and P. They noticed that the corrosion resistance, initially increasing with the anodizing potential, weakens at potentials of around 250 V. In turn, Chukwuike et al. [12] analyzed a cost-effective wet chemical method of surface treatment of niobium metal for the study of the metastable oxide film (Nb_2O_5) formed during 24 h in different media such as NaCl, NaOH, HCl, and H_2SO_4 solutions. They confirmed a time-dependent formation and dissolution of a protective oxide layer in all the tested media at different potentials. They observed a marked decrease in the corrosion rate of niobium in a 3.5 % NaCl solution after chemical formation of Nb_2O_5 layers in HCl, NaCl, and NaOH. Niobium exhibits strong corrosion properties, as well as biocompatibility comparable to titanium (Fig. 1) [23], but also low hardness [10,16], thus justifying the need for further work on improving these properties, which can be achieved through surface engineering methods. Thermal generation of oxide layers on niobium can lead to even greater improvements in corrosion resistance and surface hardness. However, due to the low mechanical properties of its core, biocompatible niobium with an oxide layer would rather find application for implants that do not have to carry much load.

The main objective of the present study was to produce niobium oxide layers by thermal oxidation of pure niobium in air and to select the material with the best mechanical, corrosion and also hydrophilic properties, i.e. with the highest potential for use on implants. In addition, the aim was also to investigate the effect of the niobium oxidation temperature on the thickness of the produced layers, their phase composition, surface roughness, hardness, wettability and corrosion resistance.

2. Experimental details

Niobium of 99.9 % mass purity in the form of 20 × 20 × 4 mm^3 specimens was used for the study. The test surfaces were ground using SiC abrasive papers with gradations from 240 to 1200, polished using a diamond slurry with a grain size of 1 μm, and then degreased in acetone using an ultrasonic cleaner. In the next step, four thermal processes of

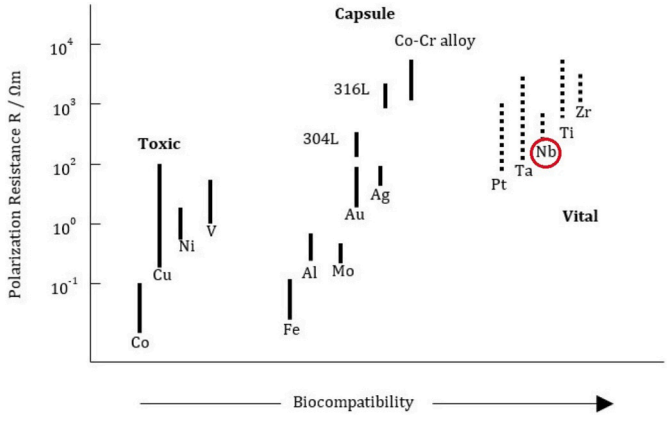

Fig. 1. Relationship between polarization resistance and biocompatibility of metals and alloys [23].

niobium oxidation were carried out at different temperatures from 400 to 500 °C. The processes' parameters are listed in Table 1. After oxidation, the samples were cooled together with the furnace. The processes were carried out in a model RS 80/300/13 Nabertherm furnace. Microstructural examinations were carried out using a Hitachi S-3500N scanning electron microscope (SEM). The microscope was primarily used to determine the thickness of the oxidised layers. For this purpose, the samples were first sectioned, after which the cut surfaces were ground and polished in the same way as the sample surfaces were prepared for the oxidation processes. Using SEM, the surface morphology of the produced layers was also evaluated. An analysis of the oxygen content at five points on the surface of the layers for each variant was also performed, along with imaging of the distribution map of niobium and oxygen on their cross-sections, using a ThermoNoran energy-dispersive EDS X-ray spectroscope equipped with a Hitachi S-3500N scanning electron microscope. Analyses were performed at a voltage of 10 kV, which allowed the accelerated electron beam to penetrate niobium and oxidised layers to a depth of ca. 500 nm. Surface roughness was examined using a WYKO NT9300 optical profilometer at 10× magnification. Five surface roughness measurements were taken each, which made it possible to calculate the average values of the parameters Ra (arithmetic mean deviation of the profile from the mean line) and Rz (sum of the average height of the five highest elevations above the mean line and the average depth of the five lowest depressions below the mean line) in Vision software. An analysis of the phase composition of niobium and the produced layers was carried out using a Bruker D8 Advance X-ray diffractometer. For niobium in the initial state, diffraction was performed in Bragg-Brentano geometry. In turn, for samples after oxidation, grazing incidence angle diffraction was used at an incident X-ray beam angle of 2° in order to enable analysis of thin films. A detailed description of the method is presented in another paper [24]. A $CuK_{\alpha 1}$ tube with a wavelength of $\lambda = 1.5406$ Å was used. X-ray patterns were performed at a 2θ range of 15° to 100°, 40 kV voltage, 40 mA current, a step of Δ2θ–0.05°, and a counting time of 3 s. The test results were compiled and analyzed using Bruker's EVA software. Based on the determined interplanar distances d_{hkl}, the lattice parameter *a* of the niobium unit cell in the initial state and after oxidation was calculated using the relation $1/d_{hkl}^2 = (h^2 + k^2 + l^2) / a^2$ for the regular system. Distortion of the lattice in the produced layers were calculated according to the formula $\varepsilon = \Delta a/a_{Nb}$ (%), where $\Delta a = a_{Nb(O)} - a_{Nb}$, a_{Nb} - lattice parameter for niobium, $a_{Nb(O)}$ - lattice parameter for oxide layer. A Shimadzu HMV-G Vickers hardness tester was used to evaluate the microhardness of the materials. Measurements were carried out on each sample at four loads: 0.490 N, 0.981 N, 1.961 N and 4.903 N. Seven indentations were made on each sample under each load. The contact angle was also tested using an automatic Rame-Hart Instrument co. goniometer, model 90-U3-PRO. Distilled water droplets were measured using DROPimage software. A total of 5 measurements were taken on each sample. The corrosion resistance of niobium and the oxide layers was tested by the potentiodynamic method in non-deoxygenated Ringer's solution (8.6 g NaCl, 0.3 g KCl, 0.333 g $CaCl_2$) at 37 °C using an Atlas-Sollich series 160221 potentiostat. The sample and solution vessel were heated to 37 °C in a POL-EKO-APARATURA laboratory incubator, model CLN 15 STD. A three-electrode system was used for the tests, with the sample being used as the test electrode, an Ag/AgCl electrode as the reference electrode, and a platinum wire as the auxiliary

Table 1
Parameters of niobium oxidation processes.

Temperature [°C]	Time [h]	Heating rate [°C/min]	Gases	Pressure
400 425 450 500	4	10	Air	Atmospheric

electrode. Prior to testing, the materials were held in open circuit potential for 2 h, which allowed stabilization of the potentials and determination of E_{ocp} values. Afterwards, the anodic polarization curves of the tested materials were recorded using the potentiodynamic method. The samples were polarised from a potential 250 mV lower than the E_{ocp} potential to a potential of 3000 mV. A polarization rate of 0.2 mV/s was applied in the potential range of ±250 mV from the E_{ocp} potential, 1 mV/s in the range up to 700 mV, and then 3 mV/s up to 3000 mV. From the obtained polarization curves, corrosion current densities i_{corr} and corrosion potentials E_{corr} were determined using the Tafel extrapolation method, R_{pol} polarization resistance values using the Stern method, and passive state current densities at a potential value of 400 mV were evaluated as well. For each variant, at least 3 measurements were made in open circuit potential and using the potentiodynamic method.

3. Results and discussion

In order to evaluate the thickness of the produced layers, cross-sectional images of the samples were taken using SEM (Fig. 2). After oxidation at 400 °C and 425 °C, no layers were observed on the cross-section (Fig. 2a,b). Only at 450 °C did an even layer form, but transverse cracks were visible nevertheless (Fig. 2c). In turn, at 500 °C, a layer was formed in which parallel cracks and pores were present (Fig. 2d). It is noted that the amount of defects in the layer increases significantly with increasing temperature (≥450 °C). The thicknesses of the visible layers formed by oxidation at 450 °C and 500 °C were measured. The average thickness of the layer formed at 450 °C was 22.56 ± 0.04 μm, while at 500 °C it was more than two times less, i.e. 9.95 ± 1.22 μm. The significant decrease in thickness is due to surface degradation, which is a result of niobium's low heat resistance. Part of the layer chipped off after the oxidation process. When the treated samples were removed from the furnace, a significant portion of the oxides was observed to separate from the surface. The increase in oxidation temperature contributed to increased oxygen diffusion and possibly stresses in the layer, which contributed to its chipping. The greater measurement error of the layer thickness after the process at 500 °C, compared to the sample oxidised at 450 °C, is the result of the formation of an uneven, porous and brittle layer.

Surface tests were performed to evaluate the layers' morphology (Fig. 3). In the initial state, defects caused by mechanical grinding and polishing of the surface can be seen (Fig. 3a). After oxidation at 400 °C, the surface is very similar in appearance to the initial state, with polishing defects also observed on the surface (Fig. 3b). It is only at 425 °C that a clear change in morphology is noted, where a very thin oxide layer started to form on the surface (Fig. 3c), which was not observed on the cross-section (Fig. 2b). Fig. 3c shows the discontinuities of the structure present on the surface. At 450 °C, a solid layer with a characteristic homogeneous, fine-crystalline, globular structure formed (Fig. 3d). In the case of the sample surface oxidised at 500 °C, an uneven and developed layer surface is observed, which formed as a result of degradation (Fig. 3e). Fig. 3e shows separations also visible in the cross-section (Fig. 2d), which were caused by the high brittleness of the layer produced at this temperature.

For niobium in the initial state after polishing, the Ra parameter value was 0.141 μm, while the Rz parameter amounted to 2.071 μm (Table 2). After oxidation at 400 °C and 425 °C, these values did not increase significantly. Images of their surfaces (Fig. 3b,c) confirm a similar topography to niobium in the initial state (Fig. 3a), especially for the layer oxidised at 400 °C, where the Ra and Rz parameters were 0.179 μm and 2.750 μm, respectively (Table 2). The increase in Ra parameters to 0.200 μm and Rz to 3.165 μm after the process at 425 °C is explained by the change in surface morphology (Fig. 3c). It was only at 450 °C that a significant increase in roughness was noticed due to a substantial development of the material's surface, associated with the formation of a fine-crystalline structure of the oxides (Fig. 3d). Ra and Rz values were 0.881 μm and 12.759 μm, respectively (Table 2). The highest increase in the average values of the two studied parameters compared to the results obtained at lower temperatures occurred at 500 °C; the Ra value came to as much as 2.444 μm, while the Rz value reached 28.787 μm. Compared to the layers produced at 400 and 425 °C, this increase was over a dozen times higher, while compared to the layer obtained at 450 °C, it was several times higher. Fig. 3e shows significant irregularities in the surface of the layer oxidised at 500 °C, which, as

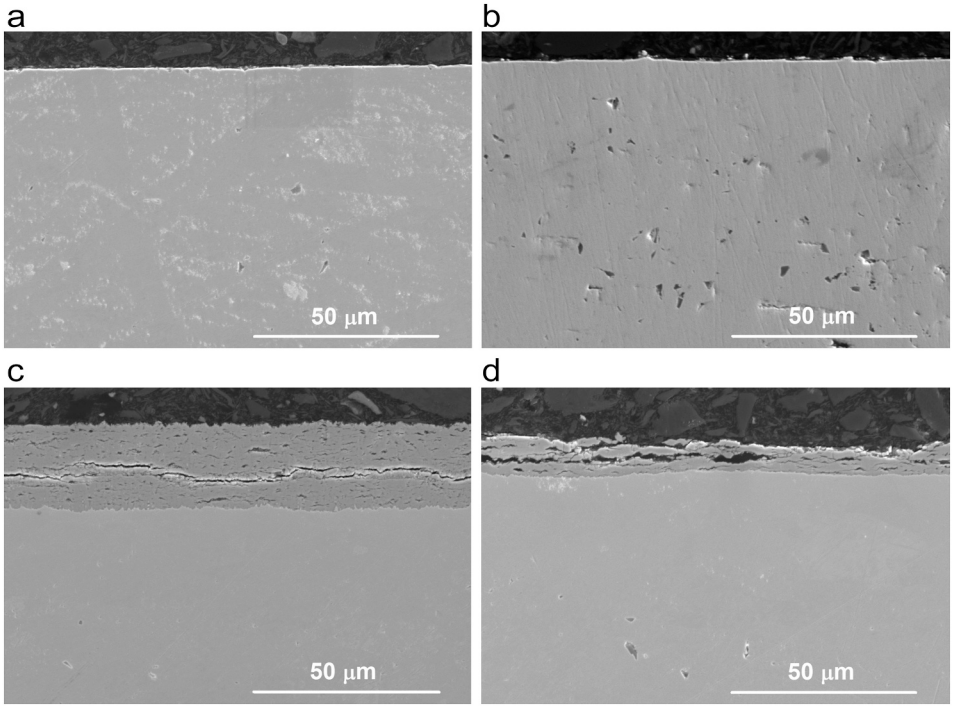

Fig. 2. SEM images of the cross-section of niobium oxidised at a) 400 °C, b) 425 °C, c) 450 °C, d) 500 °C.

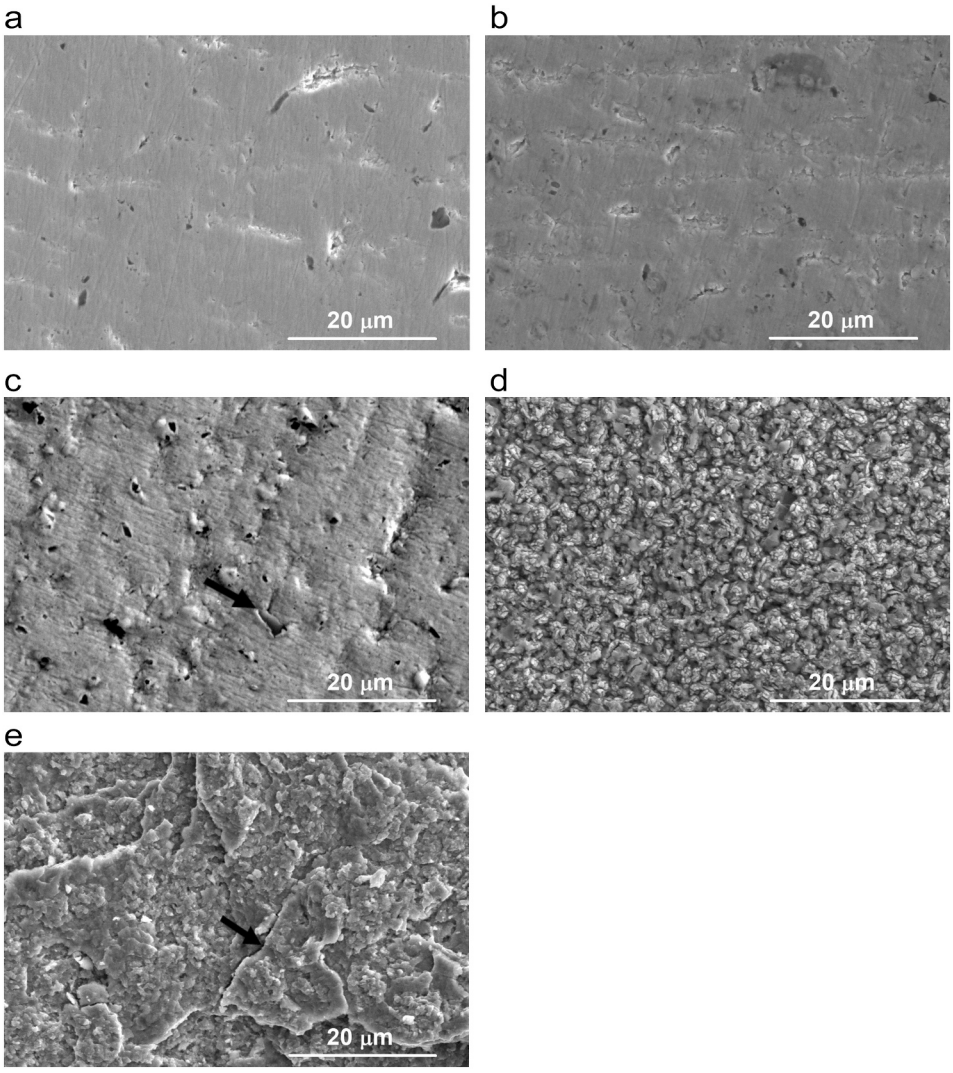

Fig. 3. SEM images of the surface of a) niobium and layers oxidised at b) 400 °C, c) 425 °C, d) 450 °C, e) 500 °C.

Table 2
Roughness of niobium and layers oxidised at 400 °C, 425 °C, 450 °C and 500 °C.

Materials	Ra [μm]	Rz [μm]
Nb	0.141 ± 0.003	2.071 ± 0.025
400	0.179 ± 0.003	2.750 ± 0.019
425	0.200 ± 0.001	3.165 ± 0.082
450	0.881 ± 0.003	12.759 ± 0.180
500	2.444 ± 0.098	28.787 ± 2.069

already stated, was due to significant chipping of the layer. Consequently, increasing the oxidation temperature contributes to an increase in the Ra and Rz parameters. In the case of layers oxidised at 400, 425 and 450 °C, the increase in roughness is attributed to the oxide morphology shaped in the oxidation processes, while in the process conducted at 500 °C, the significant development of the surface is caused by layer degradation.

X-ray patterns before and after the niobium oxidation process are shown in Fig. 4. In the initial state, a single-phase material was identified, and peaks belonging only to niobium with a regular body-centred cubic (bcc) structure were observed (Fig. 4a). The diffraction pattern shows peaks corresponding to the following crystallographic planes as viewed from the lowest 2θ angles: (110), (200), (211), (220) and (310). At 400 °C, only niobium peaks are also visible, however, they are shifted toward the lower 2θ angles (Fig. 4b). The bcc cell parameter increased to 3.363 Å after this process compared to 3.303 Å for niobium in the initial state, resulting in a 1.8 % deformation of the niobium lattice. At 425 °C (Fig. 4c), in addition to the peaks belonging to niobium, the diffraction pattern revealed peaks of very low intensity from the (001) and (180) planes belonging to orthorhombic niobium pentoxide Nb_2O_5. The peaks originating from niobium were also shifted toward lower 2θ angles in this case, and the lattice parameter was 3.370 Å, which corresponds to a 2 % lattice deformation relative to niobium in the initial state. The results indicate that for the processes carried out at 400 and 425 °C, a diffusion layer was formed, consisting of a solid solution of interstitial oxygen in niobium Nb(O) with a larger lattice parameter than niobium in the initial state. A similar mechanism is observed in the case of low-temperature nitriding or carburizing of austenitic steel, where, during the process, the so-called S phase [25–28] constituting an interstitial solution of nitrogen or carbon in austenite is formed in the face-centred cubic lattice of the surface layer, which also shows an increased lattice parameter and unit cell deformation, leading to higher corrosion resistance and hardness compared to the substrate [29]. While the 400 °C process only produced a niobium-oxygen solution Nb(O), the 425 °C process produced an outer layer of Nb_2O_5 in addition to the Nb(O) solution. In turn, oxidation of niobium for 4 h at 450 °C (Fig. 4d) and 500 °C (Fig. 4e) produced layers consisting of niobium pentoxide $Nb_2O_5$with a orthorhombic structure. At 450 °C, three main peaks with the highest

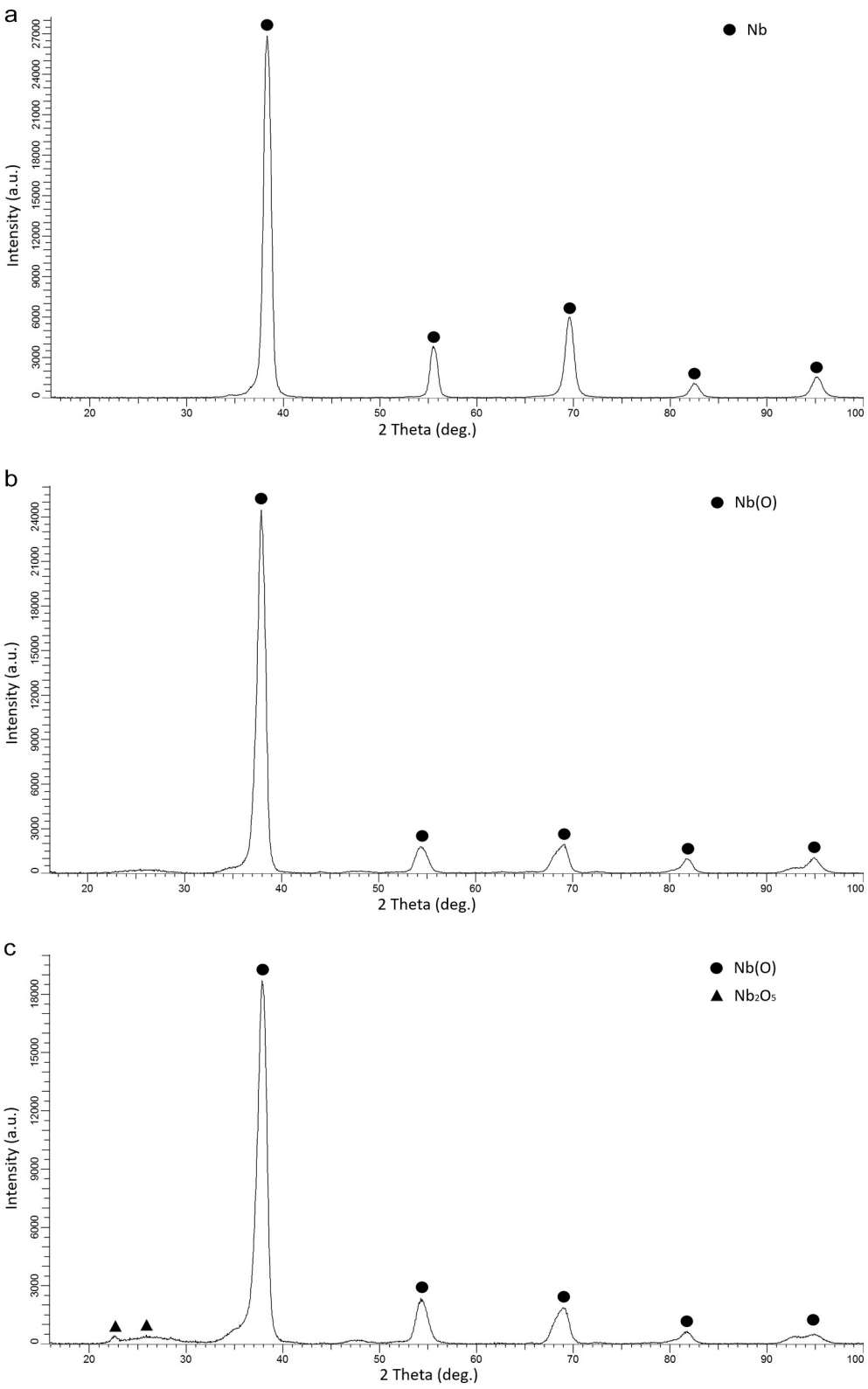

Fig. 4. X-ray diffraction patterns of a) niobium and layers oxidised at b) 400 °C, c) 425 °C, d) 450 °C, e) 500 °C.

intensity can be seen located at 2θ angles of 22.61°, 28.40° and 36.60° and corresponding to the planes (001), (180) and (181). At 500 °C, a reduction in the intensity of the peaks originating from planes (001) and (181) is apparent compared to the layer formed at 450 °C. It is likely that at this temperature a structure is formed in which the Nb_2O_5 phase with the (180) plane predominates, or the degradation of the layer at this temperature has resulted in the uncovering of an inner layer composed of an oxide showing mainly a structure characterised by the above crystallographic plane. It should be mentioned that after processes at higher temperatures (450 °C, 500 °C), in addition to Nb_2O_5, an internal

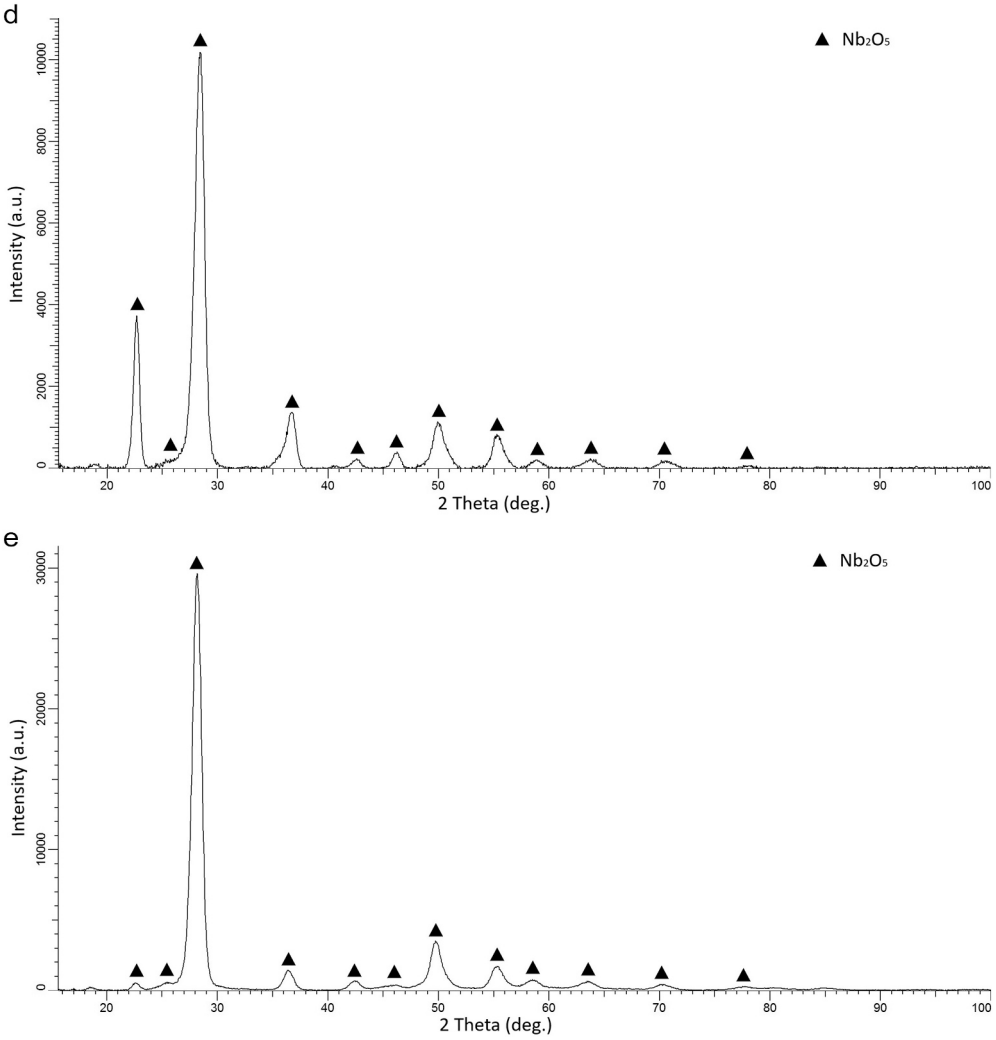

Fig. 4. (*continued*).

Nb(O) diffusion layer could also be formed, however, the applied CuKα radiation did not make it possible to obtain a signal from such a deep zone. Based on the analyses, it can be concluded that the selection of an appropriate temperature in the thermal method provides great opportunities for controlling the phase composition of oxide layers produced on niobium, which cannot be guaranteed using chemical and electrochemical methods [12,13].

In the initial state, the average oxygen content on the niobium surface was 11.7 at.% (Table 3), which is due to the presence of the passive layer. Oxidation even at the lowest temperature (400 °C) contributed to an increase in oxygen content by more than three times. At 425 °C, the oxygen content of the layer increased by another 3.3 at.%, which also translated into an increase in the lattice parameter. The use of an accelerating voltage of 10 kV in the case of niobium enables analysis up to a depth of about 500 nm, which means that the beam depth does not exceed the thickness of the layers obtained (Fig. 5). Most of the oxygen diffused into the niobium surface layer at 500 °C and was as high as 48.2 at.%. This is mainly linked to the increase in the rate of oxygen diffusion into the body-centred cubic lattice structure of niobium as the oxidation temperature increased. The EDS method shows lower accuracy in the measurement of light elements, however, the obtained results reveal a clear trend of increasing oxygen content with increasing oxidation temperature. An increase in oxygen concentration in the niobium surface layer contributes to an increase in residual stress. This effect has a significant impact on hardness (Fig. 6) and also on the durability of the layers. Exceeding a certain amount of diffusing oxygen at a temperature of 450 °C causes a critical increase in residual stress, which leads to the first cracks in the layer (Fig. 2c) followed by catastrophic cracking at 500 °C (Fig. 2d).

Table 3
Chemical composition [at. %] measured on the surface of niobium and layers oxidised at 400 °C, 425 °C, 450 °C and 500 °C.

Materials	O	Nb
Nb	11.7 ± 0.6	88.3 ± 0.6
400	39.3 ± 1.4	60.7 ± 1.4
425	42.6 ± 0.3	57.4 ± 0.3
450	47.1 ± 4.1	52.9 ± 4.1
500	48.2 ± 1.1	51.8 ± 1.1

Fig. 5 illustrates an elemental distribution map on the cross-section of the layers for each niobium oxidation temperature. In each case, niobium depletion and enrichment in oxygen is observed in the surface layer. At 400 °C (Fig. 5a), the amount of diffused oxygen in the niobium surface layer is the smallest compared to the processes carried out at higher temperatures (Table 3). Oxygen distribution imaging made it possible to estimate the thickness of the layer of the niobium-oxygen solid solution Nb(O) produced at 400 °C and of Nb_2O_5 + Nb(O) at 425 °C. The thicknesses were similar (ca. 0.7 μm) but a noticeable difference in the intensity of oxygen distribution at the cross-section was observed (Fig. 5a,b). Increasing the process temperature by as much as

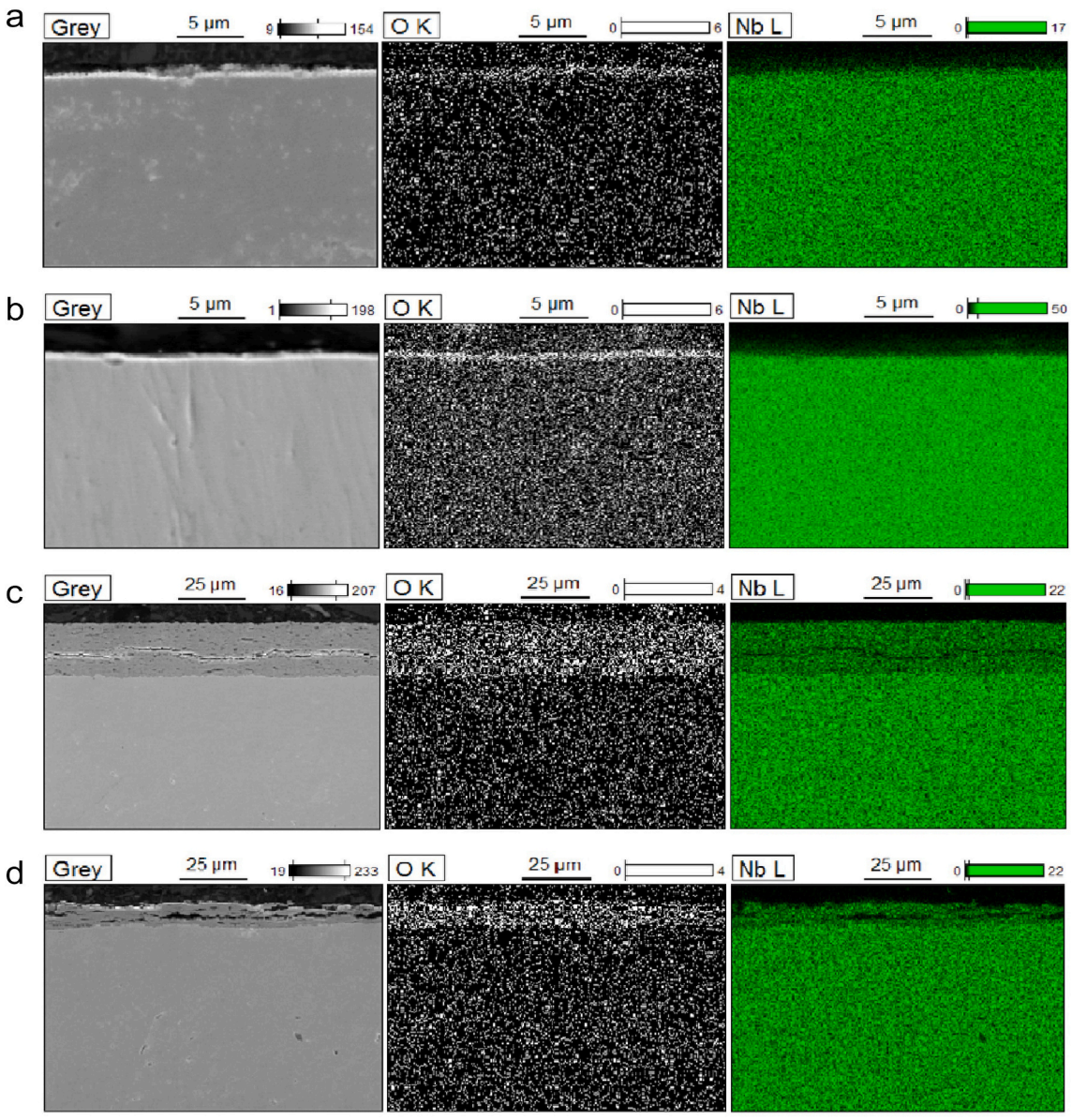

Fig. 5. Oxygen and niobium distribution on the cross-section of layers oxidised at a) 400 °C, b) 425 °C, c) 450 °C, d) 500 °C.

25 °C leads to a significant change in the film structure, where a transition is observed in this temperature range from an interstitial solid solution structure to an Nb_2O_5 orthorhombic structure in the surface layer. The mapping of niobium distribution in the layer after the processes at 450 °C and 500 °C shows dark areas where none of the elements were detected (Fig. 5c,d), thus confirming the formation of cracks and discontinuities in these areas.

In the initial state, niobium hardness reached a maximum of 1.1 GPa (at a load of 0.490 N), while for the other loads it remained in the range of 1.01–1.08 GPa (Fig. 6). After all the oxidation processes, the hardness of the surface layers increased significantly compared to the initial state. Especially in the near-surface zones (at low loads of 0.490 N and 0.981 N), a significant increase in hardness can be observed. Increased hardness accompanies increasing process temperatures at all applied loads. The different hardness values of the produced layers are mainly linked to their phase composition, i.e. the formation of niobium pentoxide Nb_2O_5 or a niobium-oxygen solid solution Nb(O). At a process temperature of 400 °C, a thin, diffusion layer (ca. 0.7 µm) of a solid solution Nb(O) appears (Fig. 4b). This layer yields the lowest increase in hardness (2.16 GPa at load of 0.490 N) mainly because of an increased lattice parameter and

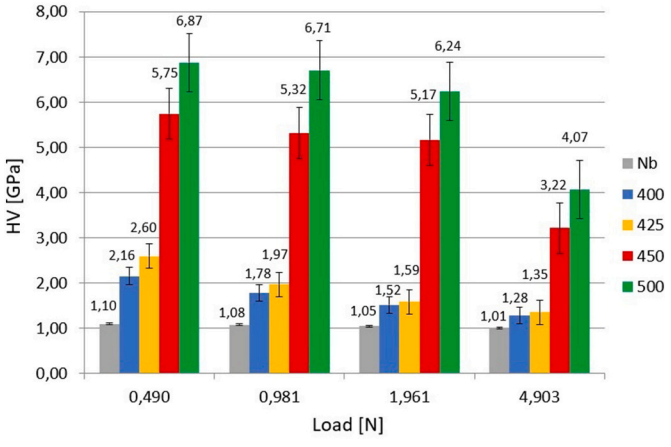

Fig. 6. Microhardness of niobium and layers oxidised at 400 °C, 425 °C, 450 °C and 500 °C.

lattice deformation. In turn, a higher hardness (2.6 GPa at load of 0.490 N) was obtained after the process at 425 °C, which was due to the presence of a thin top layer of Nb_2O_5 (Fig. 4c) and an inner layer of Nb(O) solid solution with higher lattice deformation compared to the layer produced at 400 °C. The indenter penetration depth calculations show that the applied loads did not cause its penetration to the core. All indenter depths were smaller than the layers' thicknesses. For example, in the case of the thinnest layers produced at 400 and 425 °C (ca. 0.7 μm), tested at the highest load of 4.903 N, the indentation depth did not exceed 420 nm. However, note that thin films show a soft substrate effect, which manifests itself in some decreasing microhardness with increasing indenter load. At higher oxidation temperatures (450 °C, 500 °C), the formation of a ceramic Nb_2O_5 layer (Fig. 4d,e), as well as an increase in oxygen diffusion and a resulting increase in residual stresses, caused the greatest increase in microhardness. Despite the significant degradation of the layer produced at 500 °C, its highest hardness is mainly due to the highest concentration of oxygen in this layer (Table 3). In addition, the measurement error increased as a result of significant surface development of the layers formed at ≥450 °C.

The type of surface has a direct impact on hydrophilic and hydrophobic properties, which also affect a material's biological properties. For this reason contact angle measurements were performed. Fig. 7 shows photos of droplets on the surface of niobium in the initial state and on the tested layers, while Fig. 8 gives the obtained average values of the angle between the surface of the samples and the plane tangent to the droplet surface. The water droplet on pure niobium, shown in Fig. 7a, has an average angle value of 56.3° (Fig. 8). It was observed that after oxidation at 400 °C and 425 °C, the droplets increasingly spread over the surface of the material (Fig. 7b,c). The contact angle values decreased with process temperature, resulting therefore in increased hydrophilic properties (Fig. 8). It is also noticeable that the contact angle

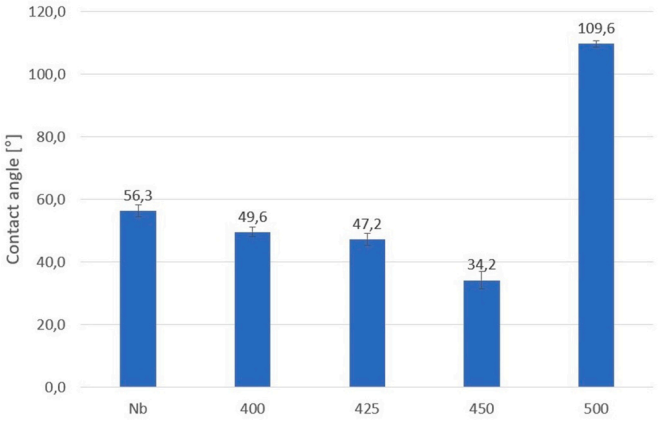

Fig. 8. Contact angle of niobium surface and layers oxidised at 400 °C, 425 °C, 450 °C and 500 °C.

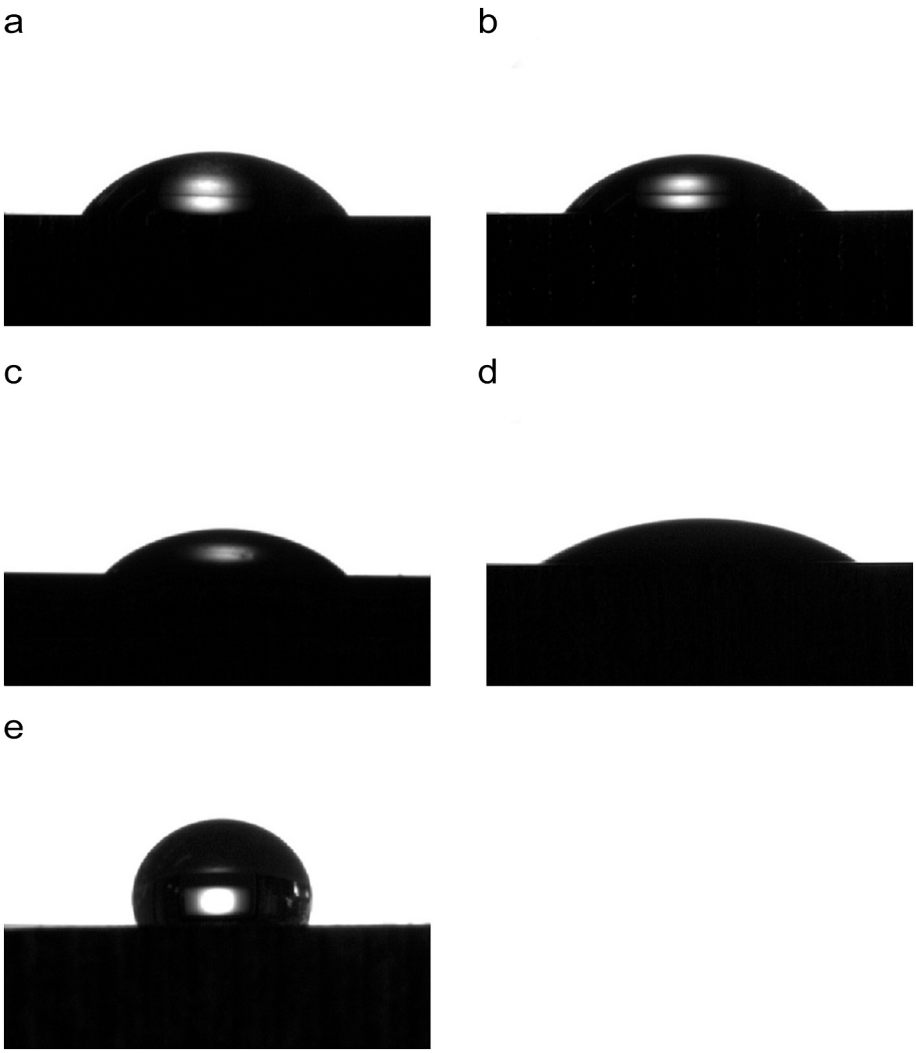

Fig. 7. Images of water droplets on the surface of a) niobium and layers oxidised at b) 400 °C, c) 425 °C, d) 450 °C, e) 500 °C.

decreased more sharply after the process at 450 °C (Fig. 7d, 8), in which a fine-crystalline structure of Nb_2O_5 oxides was formed on the layer's surface (Fig. 3d). As is well known, the increase in wettability contributes to increased cell adhesion to the material, and thus can facilitate the process of permanent bonding of the implant to the patient's bone [30]. Fig. 7e shows a droplet on the surface of niobium oxidised at 500 °C. There was an abrupt change in properties here compared to the other samples. The contact angle here reached values of a whopping 109.6 °C (Fig. 8), thereby rendering the material hydrophobic. The increase in the angle value may be due to the high surface development (Table 2). Yang et al. [15] obtained porous niobium oxide microcones, consisting of highly branched oxide nanofibers by anodizing of niobium metal in hot phosphate-glycerol electrolyte. The layers, due to their controlled but relatively large surface development, exhibited superhydrophobic properties with a contact angle reaching 175°. Layers exhibiting such a high contact angle do not have applications for implants that come into contact with human tissue, but may find use, for example, on self-cleaning windows or in the corrosion protection of metals. It can therefore be concluded that the formation of the Nb(O) diffusion layer resulted in a decrease in the contact angle, and the appearance of a very thin, uneven Nb_2O_5 layer contributed to a further fall of the contact angle. The formation of a thick, uniform at the surface, Nb_2O_5 layer caused an even greater decrease of the contact angle. In turn, the formation of an uneven, cracked, rough Nb_2O_5 layer resulted in a significant increase in the contact angle and a change into hydrophobic properties.

Using the open-circuit potential test method, the time dependence of the potential in Ringer's solution at 37 °C was determined (Fig. 9). Except for the material oxidised at 450 °C, the potential values initially increase and then all stabilise. The curves have a stable progression, and this may indicate the formation of permanent passive layers. The lowest potential values were recorded for the sample in the initial state. Oxidation at 400 °C caused the open circuit potential to shift in the positive direction. Its maximum value was 154 mV, thus showing the highest anti-corrosion properties among the samples tested in this study. At a process temperature of 425 °C, the value of the potential slightly decreased by about 20 mV compared to the 400 °C process layer, which may be due to the presence of structural discontinuities (Fig. 3c) on the surface of the Nb_2O_5 thin film (Fig. 4c). Increasing the oxidation temperature to 450 °C and also to 500 °C resulted in the formation of Nb_2O_5 layers with significant defectivity (Fig. 2c,d), which led to a decrease in the open-circuit potential to 0 mV and 30 mV, respectively, but these values are still higher than for niobium in the initial state (ca. −50 mV). Thus, in every case studied, oxidation had a positive effect on the corrosion properties of niobium. Calepa et al. [22] also tested niobium in Ringer's solution after anodic oxidation at different potentials (100, 200 and 250 V) and obtained E_{ocp} values close to 0 V for all the layers

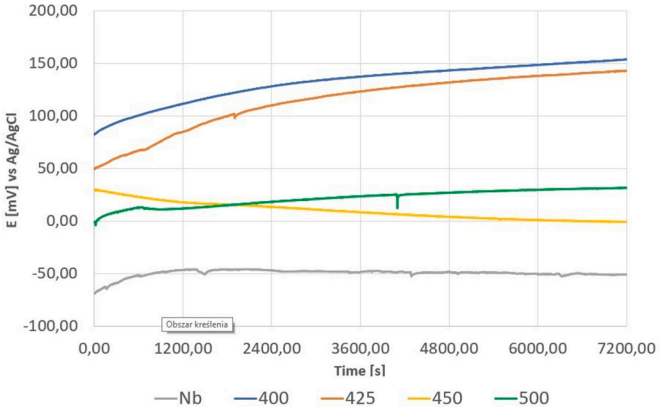

Fig. 9. Open circuit potential of niobium and layers oxidised at 400 °C, 425 °C, 450 °C and 500 °C.

produced. The layers had a thickness of ≤11 μm; however, they were porous and inhomogeneous, which may have contributed to the lower potential values compared to the layers produced in our work at 400 °C and 425 °C. Chukwuike et al. [12] observed in 3.5 % NaCl an improvement in the E_{ocp} values of Nb_2O_5 thin films chemically produced on pure niobium by immersing the material for 24 h in NaCl, HCl and H_2SO_4 solutions at room temperature, and the values ranged from −600 mV for HCl to 100 mV for H_2SO_4.

Another evaluation intended to characterise the corrosion properties of niobium was the potentiodynamic study. Fig. 10 shows a plot of polarization curves for niobium in the initial state and after oxidation processes. Based on an analysis of the anodic polarization curves, characteristic electrochemical values were determined, i.e. corrosion current density (i_{corr}), corrosion potential (E_{corr}), polarization resistance (R_{pol}) and passive state current density (i_{pass}) (Table 4). During the initial stage of anodic polarization above the corrosion potential, anodic current densities increased, which is associated with the active state, i.e. uniform corrosion, after which the current values stabilised due to passivation of the material. Again, niobium proved to be the least resistant to corrosion in the initial state with a polarization resistance of $6.5{\cdot}10^5$ Ω*cm^2. It achieved the lowest corrosion potential (E_{corr} = −140 mV), the highest passive state current density (i_{pass} = $7.5{\cdot}10^{-6}$ A/cm^2), and one of the highest corrosion current densities (i_{corr} = $1.4{\cdot}10^{-7}$ A/cm^2), compared to the layers after oxidation. On the other hand, the lowest comparable corrosion current densities i_{corr} and passive state current densities i_{pass}, and at the same time the highest values of corrosion potential E_{corr} and the highest polarization resistances R_{pol} were exhibited by samples oxidised at 400 °C and 425 °C, which respectively featured a homogeneous layer of niobium-oxygen solution Nb(O) (Fig. 4b) and a thin layer of Nb_2O_5 on Nb(O) solution (Fig. 4c). The shift of the corrosion potential E_{corr} in the positive direction, the decrease in the corrosion current density i_{corr} and the increase in the polarization resistance R_{pol} indicate a clear increase in corrosion resistance. The high value of polarization resistance R_{pol} contributing to the decrease in the magnitude of the anodic current results in a decrease in the rate of corrosion. Both materials stand out for their very high corrosion properties compared to the other materials tested, with corrosion current densities i_{corr} or passive state current densities i_{pass} being two orders of magnitude lower and polarization resistances two orders of magnitude higher than niobium in the initial state (Table 4). Canepa et al. [22] obtained polarization resistance values for anodically oxidised niobium films in the range of $0.26{\cdot}10^7$–$3.24{\cdot}10^7$ Ω*cm^2, and these values are of a similar order of magnitude to those for the films obtained in our study in processes at 400 °C and 425 °C. After oxidation at 450 °C and 500 °C, there was a significant decrease in the E_{corr} corrosion potential values of −137 mV and −76 mV, respectively, which was mainly due to the defects and discontinuities of the Nb_2O_5 ceramic layers (Fig. 2c,d). However, there was an improvement in some parameters compared to niobium in the initial state. The polarization resistance R_{pol}, which depends primarily on the corrosion current density i_{corr}, is comparable for these layers to that of niobium in the initial state; they are of the same order of magnitude. In contrast, the value of the corrosion current density i_{corr} for the layer produced at 500 °C is an order of magnitude lower compared to the initial state, and the current densities of the passive state i_{pass} for the processes carried out at 450 °C and 500 °C are an order of magnitude lower than the initial state. These results also indicate a significant decrease in the corrosion resistance of these layers compared to niobium oxidised at 400 °C and 425 °C. However, all oxidation processes had a positive influence on the corrosion properties of niobium, there was a marked improvement over pure niobium, which is most clearly seen in layers produced at the two lowest temperatures (Fig. 10, Table 4). Chukwuike et al. [12] also observed an increase in the corrosion potential E_{corr} and a decrease in the corrosion current density i_{corr} of Nb_2O_5 layers chemically produced on niobium by immersion in HCl and NaCl solutions; however, these values showed lower corrosion potentials E_{corr} and higher corrosion current densities i_{corr} likely due to different oxide formation mechanisms and

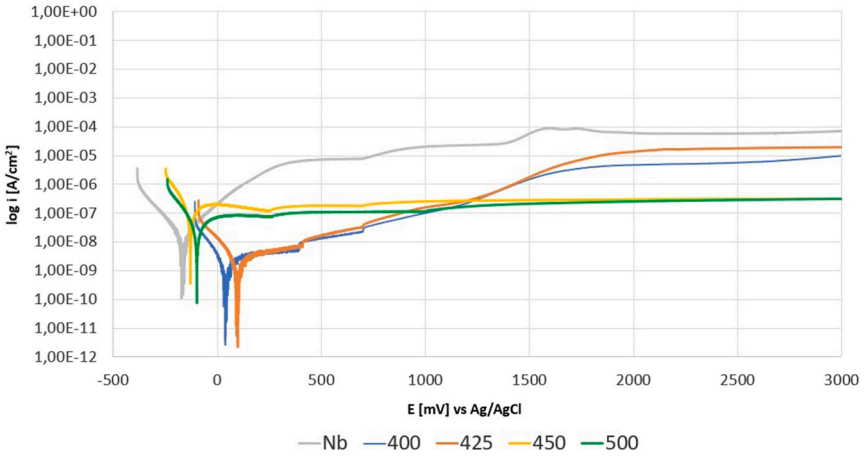

Fig. 10. Polarization curves of niobium and layers oxidised at 400 °C, 425 °C, 450 °C and 500 °C.

Table 4
Electrochemical parameters of niobium and layers oxidised at 400 °C, 425 °C, 450 °C and 500 °C.

Materials	I_{corr} [A/cm^2]	E_{corr} [mV]	R_{pol} [Ω·cm^2]	I_{pass} [A/cm^2][a]
Nb	$1.4{\cdot}10^{-7} \pm 1.1{\cdot}10^{-7}$	-140 ± 26	$6.5{\cdot}10^{+5} \pm 1.6{\cdot}10^{+5}$	$7.5{\cdot}10^{-6} \pm 1.9{\cdot}10^{-7}$
400	$5.4{\cdot}10^{-9} \pm 1.1{\cdot}10^{-9}$	73 ± 13	$1.5{\cdot}10^{+7} \pm 1.6{\cdot}10^{+6}$	$1.5{\cdot}10^{-8} \pm 1.0{\cdot}10^{-9}$
425	$2.8{\cdot}10^{-9} \pm 9.0{\cdot}10^{-10}$	74 ± 11	$1.1{\cdot}10^{+7} \pm 2.0{\cdot}10^{+6}$	$1.9{\cdot}10^{-8} \pm 1.1{\cdot}10^{-9}$
450	$2.3{\cdot}10^{-7} \pm 1.2{\cdot}10^{-8}$	-137 ± 8	$2.3{\cdot}10^{+5} \pm 9.6{\cdot}10^{+3}$	$1.5{\cdot}10^{-7} \pm 1.2{\cdot}10^{-8}$
500	$8.6{\cdot}10^{-8} \pm 6.9{\cdot}10^{-9}$	-76 ± 15	$8.7{\cdot}10^{+5} \pm 7.8{\cdot}10^{+4}$	$1.1{\cdot}10^{-7} \pm 3.1{\cdot}10^{-9}$

[a] i_{pass} measured at 400 mV.

much thinner layers compared to the Nb_2O_5 layers produced in the present work.

4. Conclusions

The effect of oxidation temperature on the properties of niobium during oxidation in an air atmosphere was evaluated. Basic tests were carried out to verify the functional properties and microstructure of the layers after thermal oxidation at 400 °C, 425 °C, 450 °C and 500 °C. The following conclusions can be drawn from the test results:

1) As per the diffraction and chemical composition analysis, oxidation conducted at 450 °C and 500 °C produced layers consisting of orthorhombic niobium pentoxide Nb_2O_5, oxidation at 400 °C produced an interstitial solution of niobium-oxygen Nb(O), while oxidation at 425 °C produced Nb(O) with a very thin surface layer of Nb_2O_5.
2) Oxidation of niobium at 450 °C and 500 °C is too intensive and contributes to surface cracking and degradation, due to its low heat resistance. After the process at 450 °C, the layer is uniform, with a fine-crystalline oxide structure on its surface, however, it cracks from the inside. In contrast, at 500 °C, despite achieving the highest hardness and good corrosion resistance, the resulting layer is inhomogeneous and has undergone significant chipping and delamination. At these temperatures, it would be advisable to apply oxidation resistant coatings on the niobium [31–35].
3) Increased oxidation temperatures result in greater hardness and roughness of niobium surfaces. Increased hardness usually results in an increase in resistance to wear by friction, and roughness in the correct range improves adhesion properties, which can have a positive effect on the cohesion of the body's tissues with the implanted material.
4) The corrosion properties and contact angle values of oxidised niobium at 400 °C and 425 °C stand out from the other results. They exhibit the highest corrosion resistance in an environment simulating body fluids. Their corrosion potential shifted toward positive values, the densities of corrosion and the passive state currents decreased by 2 orders of magnitude, while the polarization resistance increased by 2 orders of magnitude compared to the initial state. They also show hydrophilic properties, higher than those of non-oxidised niobium. The layer oxidised at 450 °C has the highest hydrophilicity and good corrosion resistance; however, due to the cracks present in its structure, it does not qualify for application. On the other hand, the layer oxidised at 500 °C also shows good corrosion resistance, although it is characterised by hydrophobic properties and significant degradation and discontinuities in the structure.

CRediT authorship contribution statement

Tomasz Borowski: Ideas, formulation of overarching research goals and aims. Development and design of methodology. Conducting a research and investigation process. Preparation and presentation of the published work, specifically writing the initial draft. Oversight and leadership responsibility for the research activity planning and execution.

Katarzyna Zielińska: Development and design of methodology. Conducting a research and investigation process. Preparation of the published work, specifically writing the initial draft.

Maciej Spychalski: Conducting a research and investigation process.

Bogusława Adamczyk-Cieślak: Conducting a research and investigation process.

Łukasz Żrodowski: Provision of study materials.

Declaration of competing interest

The authors declare that they have no known competing financial interests or personal relationships that could have appeared to influence the work reported in this paper.

Data availability

No data was used for the research described in the article.

References

[1] N. Eliaz, Corrosion of metallic biomaterials: a review, Materials 12 (2019) 407, https://doi.org/10.3390/ma12030407.

[2] H.C. Fals, L.A. Lourençato, M.S. Orozco, M.J.X. Belém, C.R.C. Lima, Slurry erosion resistance of thermally sprayed Nb2O5 and Nb2O5+WC12Co composite coatings deposited on AISI 1020 carbon steel, Ceram. Int. 46 (2020) 27670–27678, https://doi.org/10.1016/j.ceramint.2020.07.264.

[3] A. Kumar, G. Malik, R. Adalati, V. Chawla, M.K. Pandey, R. Chandra, Tuning the wettability of highly transparent Nb2O5 nano-sliced coatings to enhance anti-corrosion property, Mater. Sci. Semicond. Process. 123 (2021), 105513, https://doi.org/10.1016/j.mssp.2020.105513.

[4] J.A. Moreto, R.V. Gelamo, J.P.L. Nascimento, M. Taryba, J.C.S. Fernandes, Improving the corrosion protection of 2524-T3-Al alloy through reactive sputtering Nb2O5 coatings, Appl. Surf. Sci. 556 (2021), 149750, https://doi.org/10.1016/j.apsusc.2021.149750.

[5] M. Dinu, L. Braic, S.C. Padmanabhan, M.A. Morris, I. Titorencu, V. Pruna, A. Parau, N. Romanchikova, L.F. Petrik, A. Vladescu, Characterization of electron beam deposited Nb2O5 coatings for biomedical applications, J. Mech. Behav. Biomed. Mater. 103 (2020), 103582, https://doi.org/10.1016/j.jmbbm.2019.103582.

[6] F.R. Caliari, E. Garcia, F. Miranda, G.P. Filho, S. Sampath, Phase evolution in plasma sprayed Nb2O5 coatings, J. Eur. Ceram. Soc. 41 (2021) 5248–5257, https://doi.org/10.1016/j.jeurceramsoc.2021.04.022.

[7] S. Nagarajan, V. Raman, N. Rajendran, Synthesis and electrochemical characterization of porous niobium oxide coated 316L SS for orthopedic applications, Mater. Chem. Phys. 119 (2010) 363–366, https://doi.org/10.1016/j.matchemphys.2009.10.033.

[8] H.M. Wadullah, M. Talib Mohammed, T. Khalid Abdulrazzaq, Structure and characteristics of Nb2O5 nanocoating thin film for biomedical applications, Mater. Today Proc. 62 (2022) 3076–3080, https://doi.org/10.1016/j.matpr.2022.03.229.

[9] S.A. Pauline, N. Rajendran, Biomimetic novel nanoporous niobium oxide coating for orthopaedic applications, Appl. Surf. Sci. 290 (2014) 448–457, https://doi.org/10.1016/j.apsusc.2013.11.112.

[10] R. Olivares-Navarrete, J.J. Olaya, C. Ramírez, S.E. Rodil, Biocompatibility of niobium coatings, Coatings. 1 (2011) 72–87, https://doi.org/10.3390/coatings1010072.

[11] E. Eisenbarth, D. Velten, J. Breme, Biomimetic implant coatings, Biomol. Eng. 24 (2007) 27–32, https://doi.org/10.1016/j.bioeng.2006.05.016.

[12] V.I. Chukwuike, K. Rajalakshmi, R.C. Barik, Surface and electrochemical corrosion analysis of niobium oxide film formed in various wet media, Appl. Surf. Sci. Adv. 4 (2021), 100079, https://doi.org/10.1016/j.apsadv.2021.100079.

[13] M. Altomare, G. Cha, P. Schmuki, Anodic nanoporous niobium oxide layers grown in pure molten ortho-phosphoric acid, Electrochim. Acta 344 (2020), 136158, https://doi.org/10.1016/j.electacta.2020.136158.

[14] K. Mojsilović, J. Jovović, S. Stojadinović, R. Vasilić, Micro-second range pulsed DC plasma electrolytic oxidation on Ti and Nb, Solid State Sci. 133 (2022), 107018, https://doi.org/10.1016/j.solidstatesciences.2022.107018.

[15] S. Yang, H. Habazaki, T. Fujii, Y. Aoki, P. Skeldon, G.E. Thompson, Control of morphology and surface wettability of anodic niobium oxide microcones formed in hot phosphate–glycerol electrolytes, Electrochim. Acta 56 (2011) 7446–7453, https://doi.org/10.1016/j.electacta.2011.07.005.

[16] K. Ramachandran, Y.C. Jayakody, D.D. Jayaseelan, Oxidation behaviour and its effect on fracture toughness of niobium metal, Int. J. Refract. Met. Hard Mater. 110 (2023), 106033, https://doi.org/10.1016/j.ijrmhm.2022.106033.

[17] Mineral Commodity Summaries 2022, 2022, https://doi.org/10.3133/mcs2022.

[18] L. Sun, X. Zhang, L. Wang, H. Yu, F. Meng, T. Qi, Y. Peng, Separation and extraction of niobium from H2SO4 solution containing titanium and iron impurities, Sep. Purif. Technol. 295 (2022), 121207, https://doi.org/10.1016/j.seppur.2022.121207.

[19] A. Bleier, Colloids, in: Kirk-Othmer Encycl. Chem. Technol, John Wiley & Sons, Inc., Hoboken, NJ, USA, 2000, https://doi.org/10.1002/0471238961.0315121202120509.a01.

[20] T. Hryniewicz, K. Rokosz, H.R.Z. Sandim, SEM/EDX and XPS studies of niobium after electropolishing, Appl. Surf. Sci. 263 (2012) 357–361, https://doi.org/10.1016/j.apsusc.2012.09.060.

[21] E. Eisenbarth, D. Velten, M. Müller, R. Thull, J. Breme, Biocompatibility of β-stabilizing elements of titanium alloys, Biomaterials. 25 (2004) 5705–5713, https://doi.org/10.1016/j.biomaterials.2004.01.021.

[22] P. Canepa, G. Ghiara, R. Spotorno, M. Canepa, O. Cavalleri, Structural vs. electrochemical investigation of niobium oxide layers anodically grown in a Ca and P containing electrolyte, J. Alloys Compd. 851 (2021), 156937, https://doi.org/10.1016/j.jallcom.2020.156937.

[23] R. Yavuz, Hasan İsmail, Yamanoglu, β-Type Ti alloys for biomedical applications, Ann. Adv. Biomed. Sci. 3 (2020), https://doi.org/10.23880/aabsc-16000151.

[24] M. Witkowski, Z. Starowicz, A. Zięba, B. Adamczyk-Cieślak, R.P. Socha, O. Szawcow, G. Kołodziej, M. Haras, J. Ostapko, The atomic layer deposition (ALD) synthesis of copper-tin sulfide thin films using low-cost precursors, Nanotechnology. 33 (2022), 505603, https://doi.org/10.1088/1361-6528/ac9065.

[25] F.A.P. Fernandes, T.L. Christiansen, G. Winther, M.A.J. Somers, Measurement and tailoring of residual stress in expanded austenite on austenitic stainless steel, Mater. Sci. Eng. A 701 (2017) 167–173, https://doi.org/10.1016/j.msea.2017.06.082.

[26] A.P. Tschiptschin, A.S. Nishikawa, L.B. Varela, C.E. Pinedo, Thermal stability of expanded austenite formed on a DC plasma nitrided 316L austenitic stainless steel, Thin Solid Films 644 (2017) 156–165, https://doi.org/10.1016/j.tsf.2017.06.065.

[27] H.Y. Liu, H.L. Che, J.Y. Gao, G.B. Li, M.K. Lei, Low-pressure hollow cathode plasma source carburizing of AISI 304L austenitic stainless steel at low temperature, Surf. Coat. Technol. 442 (2022), 128548, https://doi.org/10.1016/j.surfcoat.2022.128548.

[28] G. Maistro, S. Kante, L. Nyborg, Y. Cao, Low-temperature carburized high-alloyed austenitic stainless steels in PEMFC cathodic environment, Surf. Interfaces. 24 (2021), 101093, https://doi.org/10.1016/j.surfin.2021.101093.

[29] T. Borowski, Enhancing the corrosion resistance of austenitic steel using active screen plasma nitriding and nitrocarburising, Materials 14 (2021) 3320, https://doi.org/10.3390/ma14123320.

[30] U.-W. Jung, J.-W. Hwang, D.-Y. Choi, K.-S. Hu, M.-K. Kwon, S.-H. Choi, H.-J. Kim, Surface characteristics of a novel hydroxyapatite-coated dental implant, J. Periodontal Implant Sci. 42 (2012) 59, https://doi.org/10.5051/jpis.2012.42.2.59.

[31] Y. Zhang, T. Fu, L. Yu, K. Cui, J. Wang, F. Shen, X. Zhang, K. Zhou, Anti-corrosion coatings for protecting Nb-based alloys exposed to oxidation environments: a review, Met. Mater. Int. 29 (2023) 1–17, https://doi.org/10.1007/s12540-022-01222-8.

[32] T. Fu, L. Chen, Y. Zhang, F. Shen, J. Zhu, Microstructure and oxidation resistant of Si–NbSi2 coating on Nb substrate at 800°C and 1000°C, Ceram. Int. 49 (2023) 21222–21233, https://doi.org/10.1016/j.ceramint.2023.03.252.

[33] Y. Zhang, T. Fu, J. Zhu, X. Zhang, Microstructure evolution, growth kinetics and formation mechanisms of silicon-rich NbSi2 coatings on Nb substrate, J. Mater. Res. Technol. 24 (2023) 6076–6087, https://doi.org/10.1016/j.jmrt.2023.04.222.

[34] X. Zhang, T. Fu, K. Cui, Y. Zhang, F. Shen, J. Wang, L. Yu, H. Mao, The protection, challenge, and prospect of anti-oxidation coating on the surface of niobium alloy, Coatings 11 (2021) 742, https://doi.org/10.3390/coatings11070742.

[35] F. Shen, T. Fu, Y. Zhang, Q. Gao, L. Chen, Synthesis of Si-NbSi2 coatings on Nb substrate by hot dip silicon-plating method under the various deposition temperatures, Appl. Phys. A Mater. Sci. Process. 128 (2022) 984, https://doi.org/10.1007/s00339-022-06129-0.